BIOCHEMISTRY
including biophysical chemistry & molecular biology

Article

pubs.acs.org/biochemistry

Biological and Structural Evaluation of 10*R*- and 10*S*-Methylthio-DDACTHF Reveals a New Role for Sulfur in Inhibition of Glycinamide Ribonucleotide Transformylase

Stephen Connelly,[†] Jessica K. DeMartino,[‡] Dale L. Boger,[‡,§] and Ian A. Wilson*[,†,§]

[†]Department of Integrative Structural and Computational Biology, [‡]Department of Chemistry, and [§]The Skaggs Institute of Chemical Biology, The Scripps Research Institute, 10550 North Torrey Pines Road, La Jolla, California 92037, United States

Supporting Information

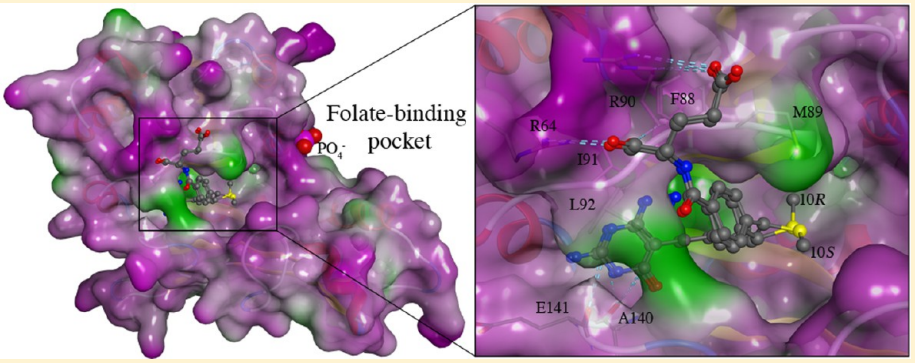

ABSTRACT: Glycinamide ribonucleotide transformylase (GAR Tfase) is a folate-dependent enzyme in the *de novo* purine biosynthesis pathway, which has long been considered a potential target for development of anti-neoplastic therapeutics. Here we report the biological and X-ray crystallographic evaluations of both independent C10 diastereomers, 10*S*- and 10*R*-methylthio-DDACTHF, bound to human GAR Tfase, including the highest-resolution apo GAR Tfase structure to date (1.52 Å). Both diastereomers are potent inhibitors (K_i = 210 nM for 10*R*, and K_i = 180 nM for 10*S*) of GAR Tfase and exhibit effective inhibition of human leukemia cell growth (IC_{50} = 80 and 50 nM, respectively). Their inhibitory activity was surprisingly high, and these lipophilic C10-substituted analogues show distinct advantages over their hydrophilic counterparts, most strikingly in retaining potency in mutant human leukemia cell lines that lack reduced folate carrier protein activity (IC_{50} = 70 and 60 nM, respectively). Structural characterization reveals a new binding mode for these diastereoisomers, in which the lipophilic thiomethyl groups penetrate deeper into a hydrophobic pocket within the folate-binding site. *In silico* docking simulations of three other sulfur-containing folate analogues also indicate that this hydrophobic cleft represents a favorable region for binding lipophilic substituents. Overall, these results suggest sulfur and its substitutions play an important role in not only the binding of anti-folates to GAR Tfase but also the selectivity and cellular activity (growth inhibition), thereby presenting new possibilities for the future design of potent and selective anti-folate drugs that target GAR Tfase.

Glycinamide ribonucleotide transformylase (GAR Tfase) is a folate-dependent enzyme in the *de novo* purine biosynthesis pathway.[1−4] GAR Tfase transfers a formyl group to the primary amine of its substrate, β-glycinamide ribonucleotide (β-GAR, **1**), through the use of the cofactor (6*R*)-N^{10}-formyltetrahydrofolic acid (10-formyl-THF, **2**) in the third step of the pathway (Figure 1). This one-carbon transfer incorporates C8 of purines and is the first of two formyl transfer reactions that leads to inosine monophosphate (IMP) and ultimately to purines.[1] The GAR Tfase mechanism has been the subject of much study in recent years for the ease with which it catalyzes the formyl transfer reaction,[5−7] its biological role in DNA precursor synthesis,[8] its role as an important target for chemotherapeutic drug design,[9−20] and, more recently, its role in *Mycobacterium tuberculosis* where it has been targeted for drug discovery.[21]

Inhibitors of folate metabolism and the enzymes responsible for the biosynthesis of nucleic acid precursors have long been considered important agents and targets for cancer chemotherapy.[22] GAR Tfase was validated more than 30 years ago as an anticancer target with the discovery of the first potent and selective inhibitor, 5,10-dideaza-5,6,7,8-tetrahydrofolic acid (DDATHF).[9] The compound was effective *in vivo* against solid murine and human tumors that did not respond to methotrexate. The potent activity of DDATHF was attributed to the reliance of tumor cells on *de novo* purine biosynthesis, whereas normal cells predominantly use salvage pathways of uridine or cytidine.[23] Lometrexol, the 6*R* diastereomer of

Received: April 25, 2013
Revised: June 27, 2013
Published: July 19, 2013

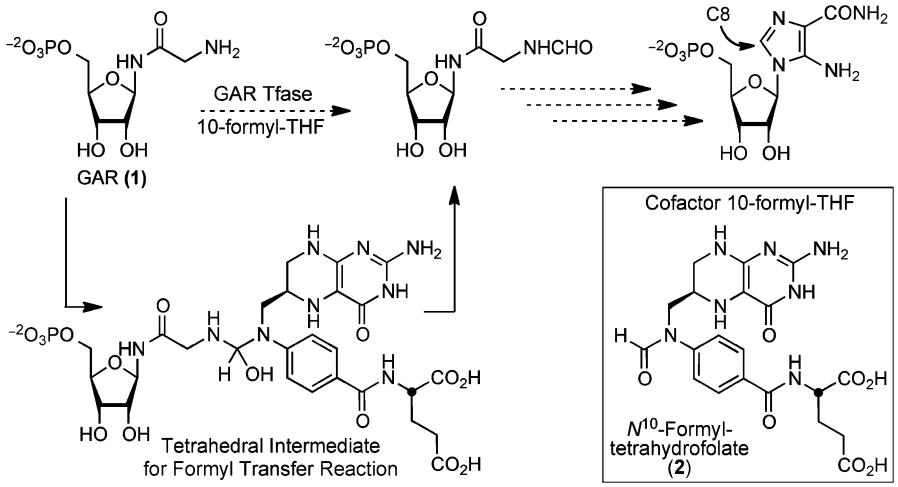

Figure 1. Formyl transfer reaction catalyzed by GAR Tfase, with the proposed tetrahedral intermediate formed between substrate β-GAR (**1**) and cofactor 10-formyl-THF (**2**).

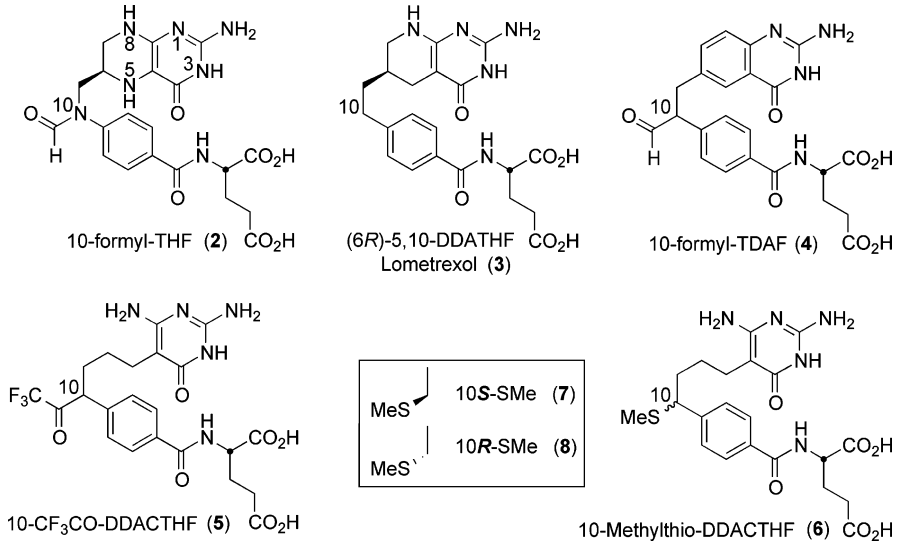

Figure 2. Chemical structures of natural cofactor 10-fTHF (**2**) and representative anti-folate analogue inhibitors.

DDATHF [**3**; K_i = 60 nM (Figure 2)], was taken forward for further clinical development. Although some patients suffered cumulative myelosuppression, which was alleviated by cosupplementation with folic acid,[24,25] Lometrexol was later withdrawn for economic reasons.

Structural biology has played a pivotal role in the design and evaluation of folate-based inhibitors for dihydrofolate reductase (DHFR),[26,27] 5,10-methylenetetrahydrofolate reductase (MTHFR),[28] thymidylate synthetase (TS),[29,30] 5-aminoimidazole-4-carboxamide-ribonucleotide (AICAR Tfase),[31−38] and GAR Tfase.[7,39−41] Previously, we reported on folate-based inhibitors that were designed to incorporate an electrophilic functional group at C10 and could potentially interact with either active site nucleophiles or the substrate amine of β-GAR to form adducts. The GAR Tfase inhibitors 10-formyl-TDAF **4**[10,40] and 10-CF_3CO-DDACTHF **5**[41,42] both contain a nontransferable formyl or trifluoroacetyl group and have proven to be potent inhibitors of GAR Tfase [K_i = 260 nM for **4**, and K_i = 15 nM for **5** (Figure 2)]. X-ray and nuclear magnetic resonance studies of both **4** with *Escherichia coli* GAR Tfase (eGAR Tfase) and **5** with human GAR Tfase (hGAR Tfase) have shown they bind as their hydrated *gem*-diols.[40,41] In both cases, the C10 center rapidly epimerizes in solution, prohibiting the evaluation of each independent diastereomer. However, the formation of these hydrophilic *gem*-diol structures mimics the formyl transfer reaction intermediate and provides strong stabilizing interactions between the inhibitor and the catalytic residues of the protein, leading to the highest-affinity inhibitors of GAR Tfase tested to date. This led to the discovery of the tetrahedral intermediate mimic[40,41] and provided a unique design feature that affords selectivity over all other folate-dependent enzymes that do not use a formyl transfer reaction.

While the effect of various substitutions at C10 was further investigated, 10*R*/*S*-methylthio-DDACTHF **6** was discovered to be a modestly potent, sulfur-containing inhibitor of hGAR Tfase (K_i = 250 nM)[17] (Figure 2). The activity of this compound, both *in vitro* and *in vivo*, was unexpected, as it does not contain the electrophilic functional group at C10 of other potent inhibitors, such as **4** and **5**. Instead, the thiomethyl moiety is a weak hydrogen bond acceptor and presents a soft hydrophobic substituent for active site binding. Despite large differences in electrostatic potentials at C10 between these inhibitors, both are able to bind to hGAR Tfase with high

dx.doi.org/10.1021/bi4005182 | *Biochemistry* 2013, 52, 5133−5144

affinity, raising important questions about the activity and selectivity that substitutions at the C10 position can confer.

Finally, although not as a C10 substitution, the incorporation of sulfur in hGAR Tfase inhibitors is already well established, with Eli Lilly's LY309887 **9**[43]and Agouron's AG2034 **10**[44] and AG2037 **11**,[45] all of which are highly potent (K_i values between 5 and 50 nM) (Figure 3). However, no crystal structures of these are available to elucidate the role of sulfur in binding of these inhibitors to hGAR Tfase.

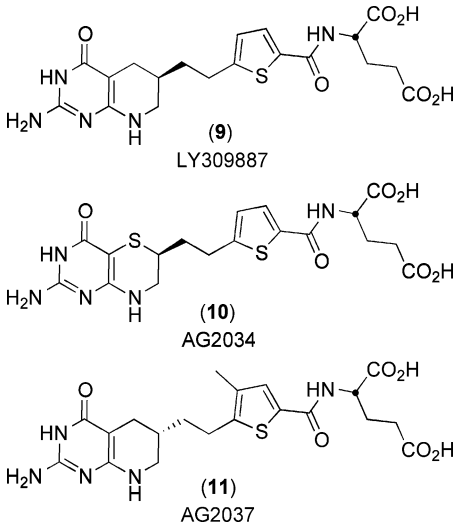

Figure 3. Chemical structures of anti-folate analogue inhibitors of hGAR Tfase that contain sulfur atoms.

The inability of the thiomethyl group to epimerize in solution was recently exploited for the successful asymmetric synthesis of **6**. This allowed for the investigation of the individual diastereomers (10*S* **7** and 10*R* **8**) in assessing the importance of C10 substitution, stereochemistry, and the contribution of sulfur to binding in this important class of hGAR Tfase inhibitors.[46] Here we report the biological and X-ray crystallographic evaluations of both independent C10 diastereomers 10*S* **7** and 10*R* **8** bound to hGAR Tfase, which reveal a new binding mode for these important anti-folates. Furthermore, to investigate the overall contribution of sulfur in binding and GAR Tfase inhibition, three other sulfur-containing folate analogues (**9**−**11**) were computationally docked into the folate-binding site of hGAR Tfase. These combined results shed light on C10 substitution, stereochemistry, and a new role for sulfur in binding within the folate-binding site of hGAR Tfase. In addition, we also provide the highest-resolution apo hGAR Tfase structure to date (1.52 Å). This high-resolution structure reveals the conformation of the previously unseen folate-binding loop and provides an excellent template for future ligand design.

MATERIALS AND METHODS

Materials. Residues 808−1010 for the hGAR Tfase domain (purN) from the native human trifunctional enzyme (purD-purM-purN) were cloned into pET22b encoding a C-terminal hexahistidine tag, as previously described.[7] Cofactor **2** was synthesized as previously described.[47] All other common reagents and buffers were obtained from Sigma-Aldrich Corp. (St. Louis, MO).

Biological Activity against hGAR Tfase and AICAR Tfase. Enzyme activity assays of recombinant hGAR Tfase and recombinant human aminoimidazole carboxamide ribonucleotide transformylase (hAICAR Tfase) were performed as previously described.[15,41] Kinetics of the enzyme reactions were monitored for 2 min after reaction initiation. All inhibition constants (K_i) were calculated using Dixon plots.

Growth Inhibition Assay. The growth inhibition activity of the compounds was measured using CCRF-CEM human leukemia cell lines as previously described.[15,41,48]

Protein Expression. Stable and soluble expression of the hGAR Tfase domain (PurN) was achieved using a transfected plasmid in BL21 (De3) *E. coli* as the expression host. Cultures (1 L) of LB containing ampicillin (100 μg/mL) were grown at 37 °C to an OD_{595} of 0.8−1.0, at which time cells were induced with 0.5 mM IPTG and incubated for a further 5 h at 30 °C.

Protein Purification. Cells were lysed using an EmulsiFlex C-3 cell disruptor (Avestin) at 15K psi and 4 °C in binding buffer [100 mM Tris, 500 mM NaCl, 40 mM imidazole, and 5 mM β-mercaptoethanol (β-Me) (pH 8.0)]. The lysate was then clarified by centrifugation at 20000*g* for 20 min at 4 °C. The clear supernatant was then passed over a 5 mL Nickel HiTrap IMAC HP column (GE Healthcare, San Diego, CA), followed by a wash of 5 column volumes of binding buffer. The bound protein was eluted by adding 1 column volume of elution buffer [100 mM Tris, 500 mM NaCl, 500 mM imidazole, and 5 mM β-Me (pH 8.0)] five times, and each fraction was analyzed by sodium dodecyl sulfate−polyacrylamide gel electrophoresis (SDS−PAGE). The hGAR Tfase-containing fractions were pooled and applied to a Superdex 75 size exclusion column (Amersham Pharmacia, Piscataway, NJ) and eluted using 20 mM Tris, 200 mM NaCl, and 5 mM DTT (pH 8.0) in 2 mL fractions. Protein purity was assessed by SDS−PAGE, and those fractions containing >95% pure protein were pooled for further use.

Crystallization and Data Collection. The hGAR Tfase was concentrated to 15 mg/mL in 20 mM Tris, 200 mM NaCl, and 5 mM DTT (pH 8.0) and was either crystallized alone or cocrystallized with inhibitors at a 5-fold molar excess (inhibitors solubilized as 500-fold stocks in dimethyl sulfoxide), using the vapor-diffusion sitting drop method. For crystallization, an equal volume (2 uL) of protein and the well condition were mixed and left to equilibrate at 4 °C. Crystals grew from 0.1 M phosphate/citrate buffer and 1.5−2.0 M ammonium sulfate (pH 4.2) with 25% (v/v) glycerol added as a cryoprotectant. All data were collected at beamline 11-1 at the Stanford Synchrotron Radiation Lightsource (SSRL) at a wavelength of 0.9795 Å. All data sets were integrated and scaled using HKL2000.[49] The diffraction data were indexed in space group $P6_522$ with one monomer per asymmetric unit and the following unit cell dimensions: $a = b = 78.2$ Å, and $c = 229.3$ Å. The Matthews coefficient[50] for each structure was approximately 4.44 Å^3/Da, which translates to a relatively high solvent content of 72%.

Structure Solution and Refinement. The structures of hGAR Tfase in both apo and ligand-bound forms were determined by molecular replacement in Phaser[51] using the previously determined low-pH structure of unliganded hGAR Tfase [Protein Data Bank (PDB) entry 1MEO][7] as the search model. Further model building and refinement were completed using Coot[52] and Refmac5,[53] respectively. After initial rounds of refinement, the locations of the inhibitors were determined from $2F^c - F^o$ omit maps (Figure S1 of the Supporting

dx.doi.org/10.1021/bi4005182 | *Biochemistry* 2013, 52, 5133−5144

Table 1. *In Vitro* hGAR Tfase and hAICAR Tfase Enzyme Inhibition and Cellular Growth Inhibition Assays[a]

	inhibition K_i (μM)		CCRF-CEM [IC_{50} (μM)]		
compound	hGAR Tfase	hAICAR Tfase	(−) T, (−) H	(+) T, (−) H	(−) T, (+) H
10*S* **7**	0.21	>100	0.05	0.07	>10
10*R* **8**	0.18	>100	0.08	0.08	>10
DDACTHF	1.7	20	2.7	3.6	>10
5	0.03	>100	0.016	0.017	>10
3 Lometrexol	0.06[b]	>100	0.2	0.2	>10

[a]Represented as K_i and *in vitro* growth inhibition as IC_{50} of human leukemia cell lines, with and without purine or pyrimidine supplementation.[46] T = thymidine, and H = hypoxanthine. [b]From ref 80.

Information). All ligand coordinates and stereochemical library files were generated using PRODRG.[54] Riding hydrogens were added and anisotropic *B* values assigned during refinement. Final resolutions and R_{cryst} and R_{free} values were 1.52 Å, 17.3%, and 19.3% for apo GAR Tfase; 1.6 Å, 17.5%, and 20.5% for GAR Tfase in complex with 10*S* **7**; and 1.7 Å, 20.1%, and 21.6% for GAR Tfase in complex with 10*R* **8**, respectively. Final models were validated using the JCSG quality control server (http://jcsgsrv2/QC) incorporating Molprobity,[55] ADIT (http://rcsb-deposit.rutgers.edu/validate), WHATIF,[56] Resolve,[57] and Procheck.[58]

***In Silico* Modeling of Sulfur-Containing hGAR Tfase Inhibitors.** Docking of the three sulfur-containing folate analogues **9**, **10**, and **11** was completed using the Dock simulation in MOE (Molecular Operating Environment 2011.10, Chemical Computing Group, Montreal, QC). The high-resolution coordinates for 10*S* **7** bound to hGAR Tfase were used as the template with the two conserved structural water molecules, which play a vital role in binding the pteridine ring,[7] being retained in the simulation. The target pocket was defined as atoms within 5 Å of the bound ligand 10*S* **7**, which was removed prior to the docking simulation. For full details of the docking methodology, see the Supporting Information.

RESULTS AND DISCUSSION

Biological Activity. Remarkably, both diastereomers of the thiomethyl derivative exhibited potent activity against hGAR Tfase, 210 nM and 180 nM for 10*S* and 10*R*, respectively (Table 1)].[46] This similarity in the activity of the two C10 diastereomers is consistent with both possessing nearly equivalent capabilities for binding at the hGAR Tfase active site. Neither isomer possessed activity against AICAR Tfase (K_i > 100 μM), suggesting the compounds act selectively on hGAR Tfase within the purine biosynthesis pathway. This selectivity appears to come directly from the C10 substitution, as the unsubstituted DDACTHF shows moderate inhibition of AICAR Tfase (K_i = 20 μM) (Table 1).[46] The compounds were also examined for the ability to suppress the growth of the human leukemia CCRF-CEM cell line (growth inhibition), in the presence (+) and absence (−) of added hypoxanthine (purine) or thymidine (pyrimidine). Both 10*S* **7** and 10*R* **8** exhibited potent activity in the cell-based assay with IC_{50} values of 50 and 80 nM, respectively, which is in line with Lometrexol **3**, with values reportedly as low as 2.9 nM[59] and in our hands here 200 nM. The activity of 10*S* **7** and 10*R* **8** is only 3−5 times less than that of **5** (16 nM), the most potent inhibitor of GAR Tfase that we tested (Table 1).[46] In the presence of thymidine, all inhibitors retained their activity, whereas the inhibitors were inactive in the presence of supplemented hypoxanthine, indicating that these compounds inhibit cell growth by selectively inhibiting an enzyme within the purine biosynthetic pathway.

Folates and anti-folates are transported into the cell through the dominant and ubiquitously expressed reduced folate carrier protein (RFC).[60] Once in the cell, they are converted to long-chain polyglutamate derivatives by folypolyglutamate synthetase (FPGS), which maximizes their cellular retention,[61] as each additional glutamate adds a negative charge that prevents interaction with the efflux pumps.[60] Mutant CCRF-CEM cell lines deficient in FPGS or the RFC were used to investigate the involvement of these proteins in regulating intracellular levels of the compounds. All of the most potent hGAR Tfase inhibitors (compounds **3**−**8**) are substrates of FPGS, as previously demonstrated by the loss of activity in cell lines that are deficient in FPGS activity (CCRF-CEM/FPGS$^-$).[10,17,41,46] When applied to these cells, both 10*R* **7** and 10*S* **8** lost ∼100-fold activity, indicating that they also benefit from intracellular polyglutamation (Table 2). Most strikingly, both 10*R* **7** and 10*S* **8** retained all of their potency in a mutant cell line deficient in RFC activity (CCRF-CEM/MTX IC_{50} values of 70 and 60 nM, respectively) (Table 2).[46] This result demonstrates that these compounds can cross the plasma membrane, even in the absence of RFC proteins, as compared to **3** (Lometrexol) and **5** that both lost activity (>100 μM).[41,42] In both mutant cell lines deficient in either FPGS or especially the RFC, the lipophilic thiomethyl-substituted DDACTHF was more potent than the unsubstituted DDACTHF or **5** containing a hydrophilic C10 substitution, highlighting the enhanced growth inhibition properties that lipophilic C10 substitutions can confer.

Table 2. *In Vitro* Growth Inhibition[a]

	(−) T, (−) H [IC_{50} (μM)]		
compound	CCRF-CEM	CCRF-CEM/FPGS$^-$	CCRF-CEM/MTX
10*S* -**7**	0.06	5	0.06
10*R* **8**	0.09	5.5	0.07
DDACTHF	2.7	>10	>100
5	0.06	>10	>100[b]
3 Lometrexol	0.2	>10	>100[b]

[a]Represented as IC_{50} in mutant human leukemia cell lines.[46] [b]From refs 41 and 42.

X-ray Structure Determination. Crystal structures were determined for apo hGAR Tfase and hGAR Tfase in complex with the independent diastereomers of 10-methylthio-DDACTHF, 10*R* **7**, and 10*S* **8**. All structures were determined between 1.52 and 1.8 Å resolution by molecular replacement using the apo hGAR Tfase structure at pH 4.2 (PDB entry 1MEO) as the search model.[7] hGAR Tfase crystallized in space group $P6_522$ with one molecule per asymmetric unit, consistent

dx.doi.org/10.1021/bi4005182 | *Biochemistry* 2013, 52, 5133−5144

Table 3. Data Collection and Refinement Statistics

	apo	10*S*-methylthio-DDACTHF	10*R*-methylthio-DDACTHF
Data Collection			
beamline	SSRL 11-1	SSRL 11-1	SSRL 11-1
wavelength (Å)	0.9795	0.9795	0.9795
resolution (Å)	1.52 (1.52−1.57)[a]	1.60 (1.60−1.66)[a]	1.70 (1.70−1.76)[a]
space group	$P6_522$	$P6_522$	$P6_522$
a, *b*, *c* (Å)	78.03, 78.03, 230.84	78.17, 78.17, 229.34	78.12, 78.12, 230.05
no. of molecules in the asymmetric unit	1	1	1
no. of observations	612892 (47021)[a]	655997 (65172)[a]	465880 (35193)[a]
no. of unique reflections	64515 (6187)[a]	55593 (5431)[a]	46588 (4512)[a]
completeness (%)	99.7 (98.4)[a]	99.9 (100)[a]	99.9 (99.7)[a]
R_{sym} (%)[b]	4.3 (58.9)[a]	4.0 (54.2)[a]	4.2 (69.6)[a]
average I/σ	42.0 (3.0)[a]	57.2 (4.0)[a]	38.3 (2.5)[a]
redundancy	9.5 (7.6)[a]	11.8 (12.0)[a]	7.8 (10.0)[a]
Refinement			
resolution (Å)	1.52−67.6	1.60−67.7	1.70−67.7
no. of reflections (working set)	61124 (4318)[a]	52652 (3807)[a]	44103 (3180)[a]
no. of reflections (test set)	3263 (229)[a]	2814 (208)[a]	2349 (172)[a]
R_{cryst} (%)[c]	17.3 (29.6)[a]	18.0 (22.2)[a]	19.9 (30.7)[a]
R_{free} (%)[d]	19.3 (33.1)[a]	21.0 (22.8)[a]	21.5 (32.8)[a]
no. of hGAR/ligand/water atoms	1532/0/217	1532/33/282	1532/33/173
no. of SO_4/PO_4 groups	3/1	2/1	2/1
average *B* value			
hGAR Tfase	19.8	18.9	22.4
ligand	no ligand	34.6	38.7
Wilson *B* value	23.7	24.8	28.9
Ramachandran plot (%)			
most favored	92.8	92.3	93.4
additionally allowed	6.6	7.2	6.6
generously allowed	0.6	0.6	0
disallowed	0	0	0
root-mean-square deviation			
bond lengths (Å)	0.018	0.017	0.018
bond angles (deg)	1.64	1.67	1.76

[a]Numbers in parentheses are for the highest-resolution shell of data. [b]$R_{sym} = \sum_{hkl}|I - \langle I\rangle|\sum_{hkl}I$. [c]$R_{cryst} = \sum_{hkl}|F_o - F_c|\sum_{hkl}F_o$. [d]$R_{free}$ is the same as R_{cryst} but for 5% of the data excluded from the refinement.

with previous structures.[7,41] The final models included residues 808−1007 from the trifunctional protein, with the last three histidines of the encoded C-terminal hexahistidine tag not being interpretable because of disorder. In previously reported hGAR structures, all contained multiple phosphate and/or sulfate ions (or phosphate and glycerol in the case of PDB entry 1MEJ).[7,41] Here one phosphate ion is seen bound in the substrate-binding pocket that mimics the phosphate moiety of substrate **1**.[7] While the sulfates have no known physiological function, their appearance here is not surprising as the protein was exposed to high concentrations of ammonium sulfate (1.5−2 M) in the crystallization experiments. All structures possess excellent stereochemical properties, and data collection and refinement statistics are listed in Table 3.

Overall Structure. The structure of hGAR Tfase can be divided into two distinct subdomains, N- and C-termini, connected through a central parallel, seven-stranded β-sheet. The N-terminal subdomain contains a Rossmann-type mononucleotide fold; at the C-terminal end of the β-sheet and positioned atop α1 is where the phosphate of the substrate β-GAR **1** would sit, and it is replaced here by an inorganic phosphate ion in the absence of substrate[7] (Figure 4A). Both the ligand-bound and apo forms of hGAR Tfase superpose almost identically across all α-carbons, suggesting ligand binding does not alter the protein conformation (Figure 4B). The overall topologies for the apo and complexed forms of hGAR Tfase are very similar to that previously reported for the apo form at pH 4.2 [PDB entry 1MEO (Figure 4C)]. Although hGAR Tfase is inactive at pH 4.2, because of conformational isomerism in the substrate-binding loop that precludes binding of substrate[7] **1**, the unliganded structure reported here at pH 4.2 and the previously determined structure at pH 8.5 (PDB entry 1MEJ) are very similar, with a root-mean-square deviation (rmsd) of 1.16 Å across all α-carbons (Figure S2 of the Supporting Information). Residues 141−146 of the folate-binding loop were absent in the previously reported low-pH, unliganded structure[7] at 1.75 Å, presumably because of disorder or conformational heterogeneity. In the higher-resolution structure presented here, we were able to model these residues revealing the conformation of this important loop at low pH (Figure 4D). However, this loop has *B* values (46 Å^2) higher than that of the rest of the protein structure (20 Å^2), reconfirming that this region is indeed very flexible. This high-resolution structure should serve as an excellent template for further drug discovery of ligands that bind to this pocket.

In both complex structures, the $2F^o - F^c$ density maps show the inhibitors bind in the folate-binding pocket with clear, strong, and interpretable electron density (Figure S1 of the

dx.doi.org/10.1021/bi4005182 | *Biochemistry* 2013, 52, 5133−5144

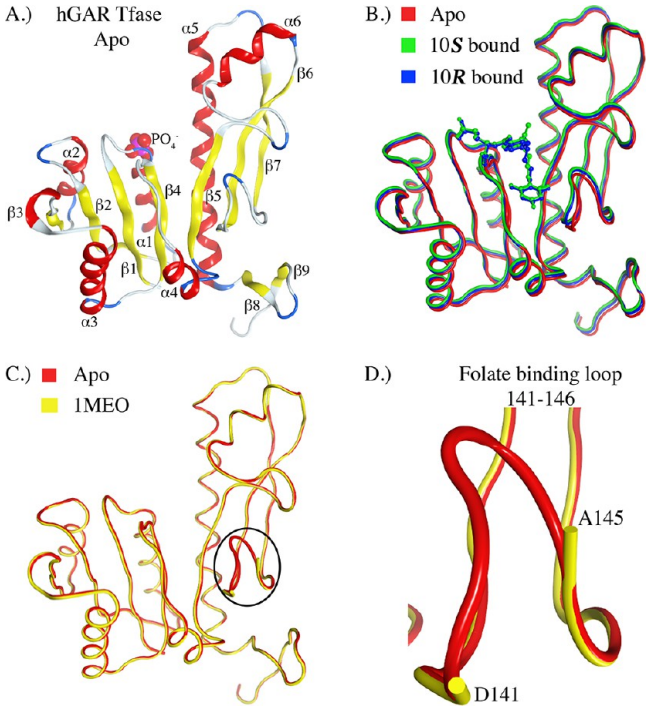

Figure 4. Crystal structure of hGAR Tfase in both apo and 10*R*- and 10*S*-methylthio-DDACTHF liganded forms. (A) Ribbon diagram of the overall topology of unliganded hGAR Tfase. Helices and β-sheets are shown as red coils and yellow strands, respectively. (B) Superposition of apo hGAR Tfase (red) with hGAR Tfase in complex with 10*S*-methylthio-DDACTHF (green) and 10*R*-methylthio-DDACTHF (blue). (C) Superposition of new high-resolution apo hGAR Tfase at 1.52 Å with the previously determined apo GAR Tfase structure at 1.75 Å (PDB entry 1MEO)[7] showing the conformation of the previously disordered folate-binding loop of residues 141−146. (D) Close-up view of the folate-binding loop of residues 141−146 as determined in the apo hGAR Tfase structure at 1.52 Å. This figure was generated using MOE 2011.10 (Chemical Computing Group).

Supporting Information). The refined *B* values of the rigid pteridine ring were similar to those of neighboring protein atoms, suggesting full occupancy of the binding site. This unambiguous electron density made it possible to resolve the structures of each individual diastereomer and investigate the importance of stereochemistry at C10. The folate-binding pocket is positioned at the interface of the N-terminal and C-terminal domains of hGAR Tfase. The binding pocket can be delineated into three parts: the pteridine-binding cleft, the formyl transfer region, and the benzoylglutamate region (described in detail below).

Pteridine-Binding Pocket. This region is responsible for the binding of the pteridine head of the natural cofactor **2**. The pteridine-binding pocket is predominantly lined with hydrophobic residues Leu85, Ile91, Leu92, Phe96, and Val97 at one end and the folate-binding loop (residues 141−146) making up the other. The diaminopyrimidinone rings of both diastereomers make a hydrogen bond between N2 of the ring and the carbonyl of the Glu141 backbone (approximately 3.1 Å) that is not seen in the quinazoline ring of **4** in complex with GAR Tfase.[40] The diaminopyrimidinone ring makes up to six hydrogen bonds to the main-chain amides and carbonyl oxygens of Arg90, Leu92, Ala140, and Glu141 and two hydrogen bonds with structurally ordered waters in a water-mediated network (Figure 5). Previous studies and *in vitro* growth inhibition experiments showed that the diaminopyrimidinone ring (seen in compounds **5**−**8**) is favored over the quinazoline ring (seen in **4**).[15] The diaminopyrimidinone ring of 10*R* **7** and 10*S* **8** contains a nitrogen atom at position N8, similar to that of natural cofactor **2** and **3** (also conserved in **9**−**11**). This ring nitrogen plays a key role in the recognition and interaction with folate binding enzymes forming one end of a hydrogen bond donor−acceptor array. Although replacement of this N8 nitrogen (for example, with carbon in **4**) does not preclude binding to hGAR Tfase, its presence has been correlated with recognition by the RFC and/or FPGS.[15] The importance of the N8 nitrogen was further demonstrated in the superior biological profile of **5** and in its complex structure (PDB entry 1NJS) in which it hydrogen bonds to the carbonyl oxygen of Arg90.[41] This important hydrogen bond (~2.8 Å) is also conserved here in both diastereomers 10*R* **7** and 10*S* **8** (Figure 5).

Formyl Transfer Region. The formyl group of natural cofactor **2** is positioned at the N10 position on the short aliphatic linker between the pteridine head and the benzoylglutamate tail. The natural cofactor **2** and ligands **3** and **4** all possess a fused bicyclic quinazoline ring system, which is replaced by the monocyclic diaminopyrimidinone in both thiomethyl diastereomers 10*R* **7** and 10*S* **8**. This monocyclic diaminopyrimidinone removes the chiral center at the C6 position and was originally designed to afford flexibility in compound **5** to optimize *gem*-diol binding with the formyl transfer region.[41] In the complex structures with **4** and **5**, hydroxyls of the *gem*-diol structures interact extensively with the formyl transfer region, primarily with Asp144 of the folate-binding loop and His108 on the β5 sheet, which are two essential residues involved in the formyl transfer reaction.[7,40,41] This interaction with the usually highly flexible folate-binding loop (Figure S3 of the Supporting Information) tethers and stabilizes the region and affords the ligand much of its extra binding capacity over **3**, which is devoid of any C10 substituent. However, the thiomethyl moiety of **6** makes no interactions with the folate-binding loop; instead, the sulfur atom is positioned deeper in a hydrophobic cleft partially occupied by the benzoyl glutamate ring (Figure 5). Application of a molecular surface colored by lipophilic potential (as calculated from the Wildman and Crippen SlogP parameters[62]) shows that this hydrophobic cleft, composed of Phe88, Met89, Ile91, and Val143, is highly lipophilic (Figure 5). Interestingly, the same flexibility designed to optimize the interaction of the *gem*-diols of the electrophile-containing compounds allows the C10 sulfur atom of both diastereomers to occupy almost identical positions here, superposing to a 0.52 Å rmsd (Figure 5). This similarity in binding mode is also reflected in the kinetic data, with each diastereomer being almost equipotent (Table 1). These data suggest that the thiomethyl positioned in this lipophilic cleft is a favorable interaction that accounts for why the ligand is able to bind to hGAR Tfase with high affinity, contrary to our initial assumptions. The position of the thiomethyl in a lipophilic cleft is consistent with previous reports in which the molecular modeling program GRID was used to predict possible binding sites for the sulfur atoms[44] and is further supported by biochemical evidence in assays where the 10*R* and 10*S* hydroxy and methoxy C10 substitutions of DDACTHF were not as potent in inhibiting hGAR Tfase.[46] The overall binding mode displayed here by both diastereomers 10*R* **7** and 10*S* **8** is distinctly different from those observed with any of the electrophile-containing analogues (Figure 6). This

dx.doi.org/10.1021/bi4005182 | *Biochemistry* 2013, 52, 5133−5144

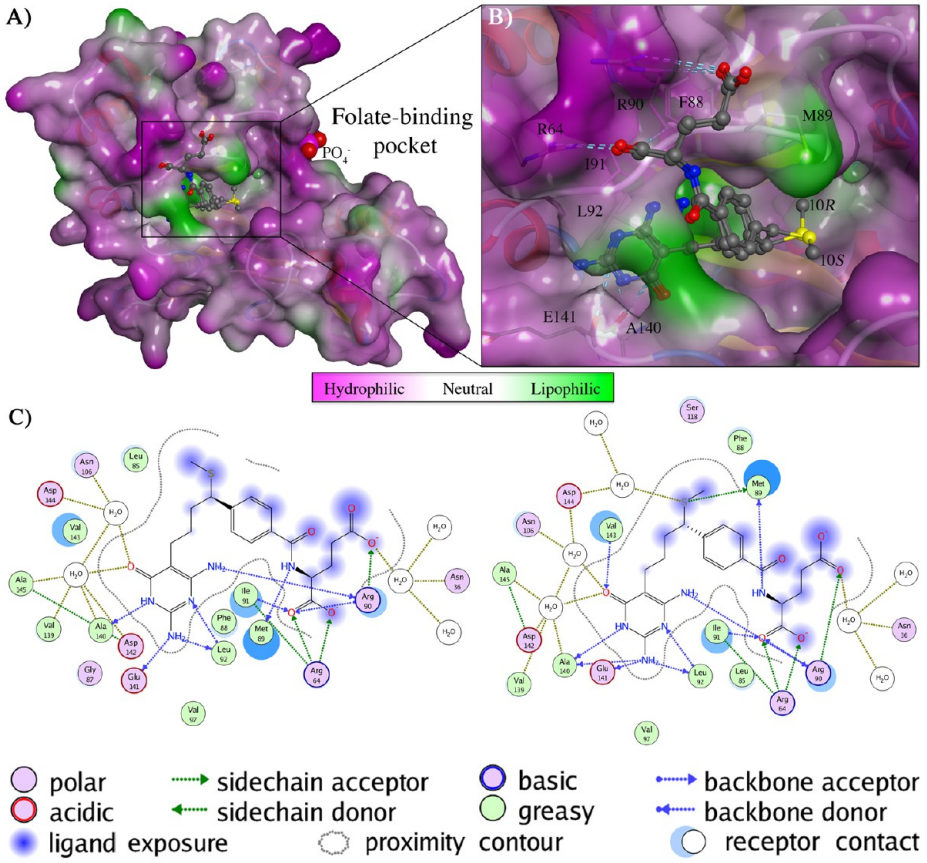

Figure 5. Structural analysis of 10*S*- and 10*R*-methylthio-DDACTHF bound to hGAR Tfase. (A) Structure of hGAR Tfase with a molecular surface applied and colored by lipophilic potential as calculated from the Wildman and Crippen SlogP parameters[62] showing the bound conformations of both 10*S*-methylthio-DDACTHF (**7**) and 10*R*-methylthio-DDACTHF (**8**) in the folate-binding pocket. (B) Close-up view of the folate-binding pocket showing the thiomethyl of 10*S*-methylthio-DDACTHF (**7**) and 10*R*-methylthio-DDACTHF (**8**) positioned in the lipophilic cleft that is lined by Phe88, Met89, Arg90, Arg91, and Leu92. (C) Schematic two-dimensional projection of the ligand interactions of 10*S*-methylthio-DDACTHF (**7**) and 10*R*-methylthio-DDACTHF (**8**) with the pteridine-binding cleft, formyl transfer region, and benzoylglutamate region of hGAR Tfase. The legend includes the amino acid type, hydrogen bond donor or acceptor origin, ligand exposure, and proximity contour of ligand−receptor contacts. Bound water molecules that mediate contacts between the ligand and receptor are also shown. This figure was generated using MOE 2011.10 (Chemical Computing Group).

highlights the complex array of binding opportunities within the hGAR Tfase folate-binding pocket that could be used to target both potency and selectivity.

Benzoylglutamate Tail Region. The biological and structural roles of polyglutamation of folates and their respective analogues are not fully known. In *E. coli* polyglutamation, there are two distinct enzymatic activities involving amide linkages through either α- or γ-carboxylates. The addition of the first two L-glutamates is catalyzed by dihydrofolate synthetase-folypolyglutamate synthetase to the γ-carboxylate. Further L-glutamate residues (4−8) are added at the α-carboxylate position by another enzyme, folypoly-α-glutamate synthetase.[63,64] The process in eukaryotes is simpler, with FPGS adding all glutamates at the γ-carboxylate.[65] The differences in the biological activities of inhibitors between the *E. coli* and hGAR Tfase can be partially explained by the observation that eGAR Tfase shows no obvious preference for the binding of the glutamate tail, which is able to switch between two distinct conformations. In eGAR Tfase complexes with both BW1476U89[66] and 10-formyl-TDAF,[40] the γ-carboxylates form salt bridges with Arg64 with the α-carboxylate facing out, whereas in an epoxide-derived, multi-substrate analogue complex structure (PDB entry 1JKX), the α-carboxylate forms the same salt bridge with the γ-carboxylate facing out.[39] It is clear that this moiety is an absolute requirement for tight binding, as previous studies showed that 10-CF_3CO-DDATHF derivatives lacking the glutamate tail are inactive against both hGAR Tfase and hAICAR Tfase.[67]

In these studies, the monoglutamate forms of 10*R* **7** and 10*S* **8** were used for both the *in vitro* testing and structural studies. The *p*-aminobenzoate ring is sandwiched within the lipophilic pocket comprised of Val143, Met89, and Phe88 and forms stacking interactions with Ile91. Although the *p*-aminobenzoate group sits deeper in the pocket than that of **5**, its conformation is consistent with previous reports in which the aromatic ring and adjacent carbonyl group are both in plane to each other.[41] In both complex structures, the glutamate makes two important conserved contacts: a salt bridge between the α-carboxylate and Arg64 and a hydrogen bond with the backbone amide of Ile91 (Figure 5). As the glutamate tail is solvent-exposed, the electron density was sufficiently clear and unambiguous for modeling of the α-carboxylate only (Figure S1 of the Supporting Information). The binding of the α-carboxylate orients the γ-carboxylate into the solvent where the density becomes weaker and disordered, consistent with the solvent-exposed, flexible nature of the polyglutamate tail.

dx.doi.org/10.1021/bi4005182 | *Biochemistry* 2013, 52, 5133−5144

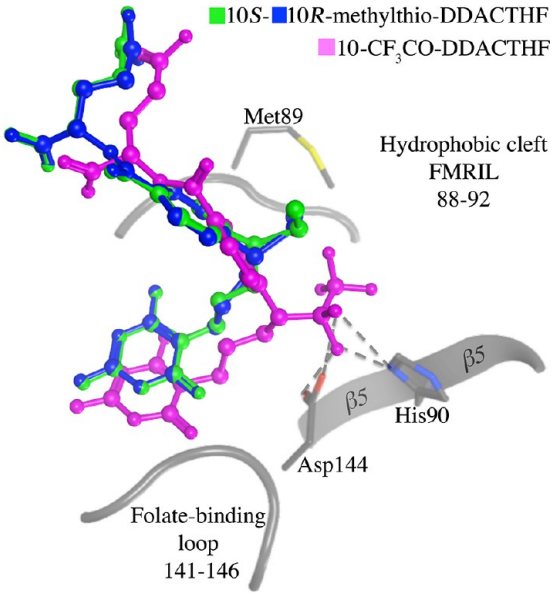

Figure 6. Superposition of bound ligand conformations of 10*S*-methylthio-DDACTHF (**7**), 10*R*-methylthio-DDACTHF (**8**), and 10-CF_3CO-DDATHF from PDB entry 1NJS (**5**) to the hGAR Tfase folate-binding site. The thiomethyl of 10*S*-methylthio-DDACTHF (**7**) or 10*R*-methylthio-DDACTHF (**8**) interacts with the lipophilic cleft consisting of Phe88, Met89, Arg90, Ile91, and Leu92, whereas 10-CF_3CO-DDATHF (**5**) interacts with Asp144 of the folate-binding loop (residues 141−146) and the catalytic His90 of strand *β*5. This figure was generated using MOE 2011.10 (Chemical Computing Group).

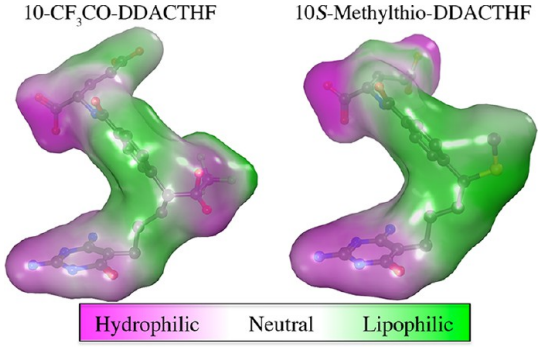

Figure 7. Structure and properties of anti-folates CF_3CO-DDATHF **5** and 10*S*-methylthio-DDACTHF **7** as bound to hGAR Tfase. Molecular surface applied and colored by lipophilic potential as calculated from the Wildman and Crippen SlogP parameters.[62] This figure was generated using MOE 2011.10 (Chemical Computing Group).

C10 Substitution and Stereochemistry. Unlike the N10 position in natural cofactor **2**, the corresponding C10 position can exist as two diastereomers, *R* and *S* (Figure 2). The most potent GAR Tfase inhibitors (**4** and **5**) both contain an electrophilic substitution at the C10 position, which bind as hydrophilic *gem*-diols mimicking the folate transfer reaction. In both cases, the C10 center rapidly epimerizes, prohibiting the evaluation of each independent diastereomer. In comparison to these transition state analogue inhibitors, the biological activity of lipophilic 10-methylthio-DDACTHF **6** was unexpected, as it does not contain the classical tetrahedral intermediate motif. Despite large differences in electrostatic potentials at the C10 position between these inhibitors (Figure 7), both were able to bind to hGAR Tfase with high affinity, raising important questions about the activity and selectivity that various substitutions at this position can confer.

To date, no structural characterization to compare individual C10 stereoisomers bound to hGAR Tfase has been reported. Analysis of $2F^o - F^c$ density maps of hGAR Tfase in complex with **4** and **5** revealed that both stereoisomers were present with **4**, whereas only one isomer was observed with **5**. Subsequent structural analysis and modeling of each isomer of **5** into the structure showed that only the *R* trifluoromethyl ketone isomer can fit, with the alternate *S* isomer sterically occluded by the loop of Asp142−Ala145 (see Figure S4 of the Supporting Information). However, the smaller hydrogen of the formyl hydrate can fit either side of this *gem*-diol structure, and hence, both isomers of **9** are observed in the $2F^o - F^c$ electron density maps.

Here, using discrete stereoisomers of 10-methylthio-DDACTHF, 10*R* **7** and 10*S* **8**, crystallographic analysis showed that both thiomethyl substituents at the C10 position were able to occupy the same position in the lipophilic cleft superposing with an rmsd of 0.52 Å. In the absence of an electrophilic group at the C10 position to interact with the folate-binding loop, the inhibitors appear to adopt a novel binding pose within the folate-binding site that places the C10 position deeper in the lipophilic cleft with no significant stereochemical preference. These structural data are consistent with previous reports supporting the preference for lipophilic C10 substitutions, whereby the corresponding hydroxy and methoxy groups were not as potent while also showing very little difference in activity between the isomers.[46]

***In Silico* Modeling of Sulfur-Containing hGAR Tfase Inhibitors.** The incorporation of sulfur in hGAR Tfase inhibitors is well-established, with compounds **9**−**11** all containing sulfur atoms in thiophene rings located between the pteridine head and glutamate tail (Figure 3). As with **3** (Lometrexol; K_i = 60 nM), inhibitors **9**−**11** also lack a C10 substitution, although they are able to bind to hGAR Tfase with higher affinity than **3** (K_i between 5 and 50 nM). However, no crystal structures are available demonstrating how these sulfur-containing inhibitors achieve high binding affinity for hGAR Tfase. To address this question, each compound was computationally docked into the folate-binding pocket of hGAR Tfase. With no C10 substitution, the overall binding orientation of each was similar to that of other folate analogue inhibitors (Figure 8 and Figures S5−S7 of the Supporting Information). In this conformation, the sulfur-containing thiophene rings of all three analogues were placed into the lipophilic cleft, consisting of residues Val143, Phe88, Met89, and Ile91. Inhibitor **10** also contains an extra sulfur atom in the pteridine ring. Docking of **10** placed the sulfur atom at the base of the pteridine-binding pocket, consisting of hydrophobic residues Leu85, Ile91, Leu92, Phe96, and Val97. Thus, the lipophilic cleft not only appears to be able to accommodate lipophilic C10 substituents but also is large enough to accept modified lipophilic ring systems in place of the *p*-benzoic acid moiety as seen with the 4-methyl-substituted thiophene ring of **11**. The placement of the sulfur atoms within these substructures into this lipophilic cleft is most likely the mechanism for which these analogues gain high-affinity binding to hGAR Tfase.

dx.doi.org/10.1021/bi4005182 | *Biochemistry* 2013, 52, 5133−5144

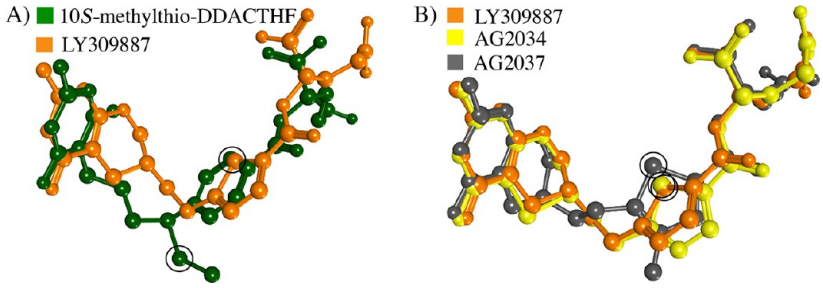

Figure 8. Comparison of bound ligand conformations with sulfur atom positions circled in black. (A) Superposition of docked LY309887 **9** and X-ray crystallographically determined 10*S*-methylthio-DDACTHF conformations as bound to hGAR Tfase **7**. (B) Superposition of the docked conformations of LY309887 **9**, AG2034 **10**, and AG2037 **11** as bound to hGAR Tfase. This figure was using MOE 2011.10 (Chemical Computing Group).

CONCLUSIONS

Herein we present the highest-resolution apo hGAR Tfase structure to date (1.52 Å) with the combined biological and structural evaluation of the two diastereomers, 10*R*- and 10*S*-methylthio-DDACTHF. Initially, the biological activity of the lipophilic C10 substitution was surprising[46] given its contrast to previous data for the requirement for hydrophilic *gem*-diols interacting with the folate-binding loop to achieve high affinity.[40,41] However, structural characterization reveals that the binding mode of both diastereomers, 10*R* **7** and 10*S* **8**, is different from that found in previous studies with electrophile-containing analogues (Figure 6). The lipophilic C10 thiomethyl penetrates deeper into a lipophilic cleft in the folate-binding site, allowing a high affinity to be achieved in the absence of interaction with the folate-binding loop observed in electrophile-containing compounds, such as **4** and **5**.[40,41]

Furthermore, *in silico* docking studies of three sulfur-containing hGAR Tfase inhibitors (**9**–**11**), which lack a C10 substituent, showed that their sulfur-containing thiophene rings also occupy this lipophilic binding cleft, suggesting a favorable site for binding of sulfur or other lipophilic moieties. A survey of other human folate-binding proteins, such as DHFR (PDB entry 1DHF),[26] TS (PDB entry 1YPV),[68] ATIC (PDB entry 1P4R),[31] methionine synthase (PDB entry 1MSK),[69] mouse serine hydroxymethyltransferase (PDB entry 1EJI),[70] and bacterial MTHFR (PDB entry 1ZP3),[71] show this lipophilic cleft to be unique to GAR Tfase. Future design considerations could use a combination of both lipophilic substitutions to afford it selectivity over other folate-dependent enzymes. The structural characterization of these sulfur-containing anti-folates has therefore shed light on the complex array of new binding opportunities in the folate-binding pocket to improve both potency and selectivity.

Folate transport and intracellular retention are also very important aspects of anti-folate design as these are actively transported into the cell through the dominant reduced folate carrier protein (RFC),[60] where they are converted to long-chain polyglutamate derivatives to increase their level of cellular retention.[61] When anti-folates are designed, the resulting compounds must be substrates of these two folate transport proteins to achieve maximal antitumor activity. It is well-established that downregulation of RFC activity is a mechanism of tumor resistance to anti-folate drugs.[72] Long-term exposure to anti-folates, such as methotrexate or pemetrexed, can also select for variants with a decreased level of expression or activity of FPGS and thereby reduce the level of retention of folates.[73,74] A study of 14 anti-folate resistant human leukemia cell lines showed most had a 90–99% loss of FPGS activity. However, because of the major contraction in cellular folate pools, these cells exhibited a marked hypersensitivity to lipid soluble anti-folates, such as neutrexin (trimetrexate) and AG377, which can cross freely into the cell.[75] The inclusion of lipophilic sulfur substituents at the C10 position has a significant effect on cellular activity, with **7** and **8** being able to retain their potency in tumor cell lines deficient in the RFC proteins. This suggests that these compounds are able to either freely pass through the membrane environment or advantageously make use of other folate pathways such as the proton-coupled mediated folate transporters (PCFT).[76] Utilizing the PCFT folate transport pathway has been seen as important in targeting solid tumors where the acidic microenvironment results in optimal PCFT activity and folate transfer rates versus that of the RFC.[77] Recently, a novel series of 6-substituted classical pyrrolo[2,3-*d*]pyrimidine thienoyl anti-folates were reported to target GAR Tfase and derived their potent antitumor activity through the efficient membrane transport by the PCFT.[78,79] Overall, these results suggest sulfur and/or its specific substitutions have an important role in the binding of anti-folates to GAR Tfase, in selectivity over other folate-binding enzymes, and in cellular transport and growth inhibition. These findings further improve our understanding and possibilities for design of potent and selective anti-folate drugs that target GAR Tfase in *de novo* purine biosynthesis.

ASSOCIATED CONTENT

Supporting Information

In silico docking methodology and figures illustrating omit map $2F^o - F^c$ density for **7** and **8**, superposition of apo hGAR Tfase at pH 4.2 and 8.5, comparison of possible C10 diastereomers of **5** bound to hGAR Tfase, and schematic two-dimensional projections of the ligand interactions of compounds **5** and **9**–**11**. This material is available free of charge via the Internet at http://pubs.acs.org.

Accession Codes

Atomic coordinates for the experimentally determined hGAR structures have been deposited in the Protein Data Bank and are available as entries 4EW1, 4EW2, and 4EW3.

AUTHOR INFORMATION

Corresponding Author

*E-mail: wilson@scripps.edu. Phone: (858) 784-9706. Fax: (858) 784-2980.

Funding

We are grateful for the financial support from the National Institutes of Health (I.A.W.) and the Skaggs Institute of Chemical Biology (I.A.W. and D.L.B.). J.K.D. is a Skaggs Research Fellow. We are also grateful to the Susan G. Komen for the Cure, which provided funding for a postdoctoral fellowship (to S.C., SGKBCF PDF0402775).

Notes

The authors declare no competing financial interest.

■ ACKNOWLEDGMENTS

We thank Drs. Robyn Stanfield and Xiaoping Dai in the Wilson laboratory for assistance in data collection and structure solution. Portions of this research were conducted at the Stanford Synchrotron Radiation Lightsource, a national user facility operated by Stanford University on behalf of the U.S. Department of Energy, Office of Basic Energy Sciences. The SSRL Structural Molecular Biology Program is supported by the Department of Energy, Office of Biological and Environmental Research, the National Institutes of Health, National Center for Research Resources, Biomedical Technology Program, and the National Institute of General Medical Sciences.

■ DEDICATION

This paper is dedicated to Fay Connelly for her love and lifelong support; she lost her brave battle with pancreatic cancer on February 22, 2010.

■ ABBREVIATIONS

GAR Tfase, glycinamide ribonucleotide transformylase; β-GAR, β-glycinamide ribonucleotide; 10-fTHF, (6*R*)-N^{10}-formyltetrahydrofolic acid; IMP, inosine monophosphate; DHFR, dihydrofolate reductase; MTFR, 5,10-methylenetetrahydrofolate reductase; TS, thymidylate synthetase; ATIC, 5-aminoimidazole-4-carboxamide ribonucleotide; AICAR, aminoimidazole carboxamide ribonucleotide transformylase; β-Me, β-mercaptoethanol; SSRL, Stanford Synchrotron Radiation Lightsource; RFC, reduced folate carrier protein; FPGS, folypolyglutamate synthetase.

■ REFERENCES

(1) Dev, I. K., and Harvey, R. J. (1978) N10-Formyltetrahydrofolate is the formyl donor for glycinamide ribotide transformylase in *Escherichia coli*. *J. Biol. Chem. 253*, 4242−4244.

(2) Caperelli, C. A. (1989) Mammalian glycinamide ribonucleotide transformylase. Kinetic mechanism and associated de novo purine biosynthetic activities. *J. Biol. Chem. 264*, 5053−5057.

(3) Inglese, J., Johnson, D. L., Shiau, A., Smith, J. M., and Benkovic, S. J. (1990) Subcloning, characterization, and affinity labeling of *Escherichia coli* glycinamide ribonucleotide transformylase. *Biochemistry 29*, 1436−1443.

(4) Wolfenden, R. (1976) Transition state analog inhibitors and enzyme catalysis. *Annu. Rev. Biophys. Bioeng. 5*, 271−306.

(5) Shim, J. H., and Benkovic, S. J. (1998) Evaluation of the kinetic mechanism of *Escherichia coli* glycinamide ribonucleotide transformylase. *Biochemistry 37*, 8776−8782.

(6) Shim, J. H., and Benkovic, S. J. (1999) Catalytic mechanism of *Escherichia coli* glycinamide ribonucleotide transformylase probed by site-directed mutagenesis and pH-dependent studies. *Biochemistry 38*, 10024−10031.

(7) Zhang, Y., Desharnais, J., Greasley, S. E., Beardsley, G. P., Boger, D. L., and Wilson, I. A. (2002) Crystal structures of human GAR Tfase at low and high pH and with substrate β-GAR. *Biochemistry 41*, 14206−14215.

(8) Poch, M. T., Qin, W., and Caperelli, C. A. (1998) The human trifunctional enzyme of de novo purine biosynthesis: Heterologous expression, purification, and preliminary characterization. *Protein Expression Purif. 12*, 17−24.

(9) Taylor, E. C., Harrington, P. J., Fletcher, S. R., Beardsley, G. P., and Moran, R. G. (1985) Synthesis of the antileukemic agents 5,10-dideazaaminopterin and 5,10-dideaza-5,6,7,8-tetrahydroaminopterin. *J. Med. Chem. 28*, 914−921.

(10) Boger, D. L., Haynes, N. E., Kitos, P. A., Warren, M. S., Ramcharan, J., Marolewski, A. E., and Benkovic, S. J. (1997) 10-Formyl-5,8,10-trideazafolic acid (10-formyl-TDAF): A potent inhibitor of glycinamide ribonucleotide transformylase. *Bioorg. Med. Chem. 5*, 1817−1830.

(11) Boger, D. L., Haynes, N. E., Warren, M. S., Gooljarsingh, L. T., Ramcharan, J., Kitos, P. A., and Benkovic, S. J. (1997) Functionalized analogues of 5,8,10-trideazafolate as potential inhibitors of GAR Tfase or AICAR Tfase. *Bioorg. Med. Chem. 5*, 1831−1838.

(12) Boger, D. L., Haynes, N. E., Warren, M. S., Ramcharan, J., Kitos, P. A., and Benkovic, S. J. (1997) Multisubstrate analogue based on 5,8,10-trideazafolate. *Bioorg. Med. Chem. 5*, 1853−1857.

(13) Boger, D. L., Haynes, N. E., Warren, M. S., Ramcharan, J., Kitos, P. A., and Benkovic, S. J. (1997) Functionalized analogues of 5,8,10-trideazafolate: Development of an enzyme-assembled tight binding inhibitor of GAR Tfase and a potential irreversible inhibitor of AICAR Tfase. *Bioorg. Med. Chem. 5*, 1839−1846.

(14) Boger, D. L., Haynes, N. E., Warren, M. S., Ramcharan, J., Marolewski, A. E., Kitos, P. A., and Benkovic, S. J. (1997) Abenzyl 10-formyl-trideazafolic acid (abenzyl 10-formyl-TDAF): An effective inhibitor of glycinamide ribonucleotide transformylase. *Bioorg. Med. Chem. 5*, 1847−1852.

(15) Marsilje, T. H., Labroli, M. A., Hedrick, M. P., Jin, Q., Desharnais, J., Baker, S. J., Gooljarsingh, L. T., Ramcharan, J., Tavassoli, A., Zhang, Y., Wilson, I. A., Beardsley, G. P., Benkovic, S. J., and Boger, D. L. (2002) 10-Formyl-5,10-dideaza-acyclic-5,6,7,8-tetrahydrofolic acid (10-formyl-DDACTHF): A potent cytotoxic agent acting by selective inhibition of human GAR Tfase and the de novo purine biosynthetic pathway. *Bioorg. Med. Chem. 10*, 2739−2749.

(16) Varney, M. D., Palmer, C. L., Romines, W. H., III, Boritzki, T., Margosiak, S. A., Almassy, R., Janson, C. A., Bartlett, C., Howland, E. J., and Ferre, R. (1997) Protein structure-based design, synthesis, and biological evaluation of 5-thia-2,6-diamino-4(3H)-oxopyrimidines: Potent inhibitors of glycinamide ribonucleotide transformylase with potent cell growth inhibition. *J. Med. Chem. 40*, 2502−2524.

(17) Cheng, H., Chong, Y., Hwang, I., Tavassoli, A., Zhang, Y., Wilson, I. A., Benkovic, S. J., and Boger, D. L. (2005) Design, synthesis, and biological evaluation of 10-methanesulfonyl-DDACTHF, 10-methanesulfonyl-5-DACTHF, and 10-methylthio-DDACTHF as potent inhibitors of GAR Tfase and the de novo purine biosynthetic pathway. *Bioorg. Med. Chem. 13*, 3577−3585.

(18) Cheng, H., Hwang, I., Chong, Y., Tavassoli, A., Webb, M. E., Zhang, Y., Wilson, I. A., Benkovic, S. J., and Boger, D. L. (2005) Synthesis and biological evaluation of N-[4-[5-(2,4-diamino-6-oxo-1,6-dihydropyrimidin-5-yl)-2-(2,2,2-trifluoroac etyl)pentyl]benzoyl]-L-glutamic acid as a potential inhibitor of GAR Tfase and the de novo purine biosynthetic pathway. *Bioorg. Med. Chem. 13*, 3593−3599.

(19) Chong, Y., Hwang, I., Tavassoli, A., Zhang, Y., Wilson, I. A., Benkovic, S. J., and Boger, D. L. (2005) Synthesis and biological evaluation of α- and γ-carboxamide derivatives of 10-CF_3CO-DDACTHF. *Bioorg. Med. Chem. 13*, 3587−3592.

(20) Wang, L., Desmoulin, S. K., Cherian, C., Polin, L., White, K., Kushner, J., Fulterer, A., Chang, M. H., Mitchell-Ryan, S., Stout, M., Romero, M. F., Hou, Z., Matherly, L. H., and Gangjee, A. (2011) Synthesis, biological, and antitumor activity of a highly potent 6-substituted pyrrolo[2,3-d]pyrimidine thienoyl antifolate inhibitor with proton-coupled folate transporter and folate receptor selectivity over the reduced folate carrier that inhibits β-glycinamide ribonucleotide formyltransferase. *J. Med. Chem. 54*, 7150−7164.

(21) Zhang, Z., Caradoc-Davies, T. T., Dickson, J. M., Baker, E. N., and Squire, C. J. (2009) Structures of glycinamide ribonucleotide transformylase (PurN) from *Mycobacterium tuberculosis* reveal a novel dimer with relevance to drug discovery. *J. Mol. Biol. 389*, 722−733.
(22) Hagner, N., and Joerger, M. (2010) Cancer chemotherapy: Targeting folic acid synthesis. *Cancer Manage. Res. 2*, 293−301.
(23) Jackson, R. C., and Harkrader, R. J. (1981) in *Nucleosides and Cancer Treatment*, pp 18−31, Academic Press, Sydney.
(24) Laohavinij, S., Wedge, S. R., Lind, M. J., Bailey, N., Humphreys, A., Proctor, M., Chapman, F., Simmons, D., Oakley, A., Robson, L., Gumbrell, L., Taylor, G. A., Thomas, H. D., Boddy, A. V., Newell, D. R., and Calvert, A. H. (1996) A phase I clinical study of the antipurine antifolate lometrexol (DDATHF) given with oral folic acid. *Invest. New Drugs 14*, 325−335.
(25) Roberts, J. D., Poplin, E. A., Tombes, M. B., Kyle, B., Spicer, D. V., Grant, S., Synold, T., and Moran, R. (2000) Weekly lometrexol with daily oral folic acid is appropriate for phase II evaluation. *Cancer Chemother. Pharmacol. 45*, 103−110.
(26) Davies, J. F., II, Delcamp, T. J., Prendergast, N. J., Ashford, V. A., Freisheim, J. H., and Kraut, J. (1990) Crystal structures of recombinant human dihydrofolate reductase complexed with folate and 5-deazafolate. *Biochemistry 29*, 9467−9479.
(27) Oefner, C., D'Arcy, A., and Winkler, F. K. (1988) Crystal structure of human dihydrofolate reductase complexed with folate. *Eur. J. Biochem. 174*, 377−385.
(28) Pejchal, R., Campbell, E., Guenther, B. D., Lennon, B. W., Matthews, R. G., and Ludwig, M. L. (2006) Structural perturbations in the Ala → Val polymorphism of methylenetetrahydrofolate reductase: How binding of folates may protect against inactivation. *Biochemistry 45*, 4808−4818.
(29) Hardy, L. W., Finer-Moore, J. S., Montfort, W. R., Jones, M. O., Santi, D. V., and Stroud, R. M. (1987) Atomic structure of thymidylate synthase: Target for rational drug design. *Science 235*, 448−455.
(30) Montfort, W. R., Perry, K. M., Fauman, E. B., Finer-Moore, J. S., Maley, G. F., Hardy, L., Maley, F., and Stroud, R. M. (1990) Structure, multiple site binding, and segmental accommodation in thymidylate synthase on binding dUMP and an anti-folate. *Biochemistry 29*, 6964−6977.
(31) Cheong, C. G., Wolan, D. W., Greasley, S. E., Horton, P. A., Beardsley, G. P., and Wilson, I. A. (2004) Crystal structures of human bifunctional enzyme aminoimidazole-4-carboxamide ribonucleotide transformylase/IMP cyclohydrolase in complex with potent sulfonyl-containing antifolates. *J. Biol. Chem. 279*, 18034−18045.
(32) Greasley, S. E., Horton, P., Ramcharan, J., Beardsley, G. P., Benkovic, S. J., and Wilson, I. A. (2001) Crystal structure of a bifunctional transformylase and cyclohydrolase enzyme in purine biosynthesis. *Nat. Struct. Biol. 8*, 402−406.
(33) Li, C., Xu, L., Wolan, D. W., Wilson, I. A., and Olson, A. J. (2004) Virtual screening of human 5-aminoimidazole-4-carboxamide ribonucleotide transformylase against the NCI diversity set by use of AutoDock to identify novel nonfolate inhibitors. *J. Med. Chem. 47*, 6681−6690.
(34) Wolan, D. W., Cheong, C. G., Greasley, S. E., and Wilson, I. A. (2004) Structural insights into the human and avian IMP cyclohydrolase mechanism via crystal structures with the bound XMP inhibitor. *Biochemistry 43*, 1171−1183.
(35) Wolan, D. W., Greasley, S. E., Beardsley, G. P., and Wilson, I. A. (2002) Structural insights into the avian AICAR transformylase mechanism. *Biochemistry 41*, 15505−15513.
(36) Wolan, D. W., Greasley, S. E., Wall, M. J., Benkovic, S. J., and Wilson, I. A. (2003) Structure of avian AICAR transformylase with a multisubstrate adduct inhibitor β-DADF identifies the folate binding site. *Biochemistry 42*, 10904−10914.
(37) Xu, L., Chong, Y., Hwang, I., D'Onofrio, A., Amore, K., Beardsley, G. P., Li, C., Olson, A. J., Boger, D. L., and Wilson, I. A. (2007) Structure-based design, synthesis, evaluation, and crystal structures of transition state analogue inhibitors of inosine monophosphate cyclohydrolase. *J. Biol. Chem. 282*, 13033−13046.
(38) Xu, L., Li, C., Olson, A. J., and Wilson, I. A. (2004) Crystal structure of avian aminoimidazole-4-carboxamide ribonucleotide transformylase in complex with a novel non-folate inhibitor identified by virtual ligand screening. *J. Biol. Chem. 279*, 50555−50565.
(39) Greasley, S. E., Marsilje, T. H., Cai, H., Baker, S., Benkovic, S. J., Boger, D. L., and Wilson, I. A. (2001) Unexpected formation of an epoxide-derived multisubstrate adduct inhibitor on the active site of GAR transformylase. *Biochemistry 40*, 13538−13547.
(40) Greasley, S. E., Yamashita, M. M., Cai, H., Benkovic, S. J., Boger, D. L., and Wilson, I. A. (1999) New insights into inhibitor design from the crystal structure and NMR studies of *Escherichia coli* GAR transformylase in complex with β-GAR and 10-formyl-5,8,10-trideazafolic acid. *Biochemistry 38*, 16783−16793.
(41) Zhang, Y., Desharnais, J., Marsilje, T. H., Li, C., Hedrick, M. P., Gooljarsingh, L. T., Tavassoli, A., Benkovic, S. J., Olson, A. J., Boger, D. L., and Wilson, I. A. (2003) Rational design, synthesis, evaluation, and crystal structure of a potent inhibitor of human GAR Tfase: 10-(Trifluoroacetyl)-5,10-dideazaacyclic-5,6,7,8-tetrahydrofolic acid. *Biochemistry 42*, 6043−6056.
(42) Desharnais, J., Hwang, I., Zhang, Y., Tavassoli, A., Baboval, J., Benkovic, S. J., Wilson, I. A., and Boger, D. L. (2003) Design, synthesis and biological evaluation of 10-CF_3CO-DDACTHF analogues and derivatives as inhibitors of GAR Tfase and the de novo purine biosynthetic pathway. *Bioorg. Med. Chem. 11*, 4511−4521.
(43) Takimoto, C. H. (1997) Antifolates in clinical development. *Semin. Oncol. 24*, S18-40−S18-51.
(44) Boritzki, T. J., Barlett, C. A., Zhang, C., and Howland, E. F. (1996) AG2034: A novel inhibitor of glycinamide ribonucleotide formyltransferase. *Invest. New Drugs 14*, 295−303.
(45) Chen, Z. H., Olopade, O. I., and Savarese, T. M. (1997) Expression of methylthioadenosine phosphorylase cDNA in p16-, MTAP- malignant cells: Restoration of methylthioadenosine phosphorylase-dependent salvage pathways and alterations of sensitivity to inhibitors of purine de novo synthesis. *Mol. Pharmacol. 52*, 903−911.
(46) DeMartino, J. K., Hwang, I., Connelly, S., Wilson, I. A., and Boger, D. L. (2008) Asymmetric synthesis of inhibitors of glycinamide ribonucleotide transformylase. *J. Med. Chem. 51*, 5441−5448.
(47) Rayl, E. A., Moroson, B. A., and Beardsley, G. P. (1996) The human purH gene product, 5-aminoimidazole-4-carboxamide ribonucleotide formyltransferase/IMP cyclohydrolase. Cloning, sequencing, expression, purification, kinetic analysis, and domain mapping. *J. Biol. Chem. 271*, 2225−2233.
(48) Bigham, E. C., Hodson, S. J., Mallory, W. R., Wilson, D., Duch, D. S., Smith, G. K., and Ferone, R. (1992) Synthesis and biological activity of open-chain analogues of 5,6,7,8-tetrahydrofolic acid: Potential antitumor agents. *J. Med. Chem. 35*, 1399−1410.
(49) Otwinowski, Z., and Minor, W. (1997) Processing of X-ray diffraction data collected in oscillation mode. *Methods Enzymol. 276A*, 307−326.
(50) Matthews, B. W. (1968) Solvent content of protein crystals. *J. Mol. Biol. 33*, 491−497.
(51) Storoni, L. C., McCoy, A. J., and Read, R. J. (2004) Likelihood-enhanced fast rotation functions. *Acta Crystallogr. D60*, 432−438.
(52) Emsley, P., and Cowtan, K. (2004) Coot: Model-building tools for molecular graphics. *Acta Crystallogr. D60*, 2126−2132.
(53) Murshudov, G. N., Vagin, A. A., and Dodson, E. J. (1997) Refinement of macromolecular structures by the maximum-likelihood method. *Acta Crystallogr. D53*, 240−255.
(54) Schuttelkopf, A. W., and van Aalten, D. M. (2004) PRODRG: A tool for high-throughput crystallography of protein-ligand complexes. *Acta Crystallogr. D60*, 1355−1363.
(55) Lovell, S. C., Davis, I. W., Arendall, W. B., III, de Bakker, P. I., Word, J. M., Prisant, M. G., Richardson, J. S., and Richardson, D. C. (2003) Structure validation by Cα geometry: ϕ, ψ and Cβ deviation. *Proteins 50*, 437−450.
(56) Vriend, G. (1990) WHAT IF: A molecular modeling and drug design program. *J. Mol. Graphics 8*, 29 , 52−56.

(57) Terwilliger, T. C. (2003) Automated main-chain model building by template matching and iterative fragment extension. *Acta Crystallogr. D59*, 38−44.
(58) Laskowski, R. A., Moss, D. S., and Thornton, J. M. (1993) Main-chain bond lengths and bond angles in protein structures. *J. Mol. Biol. 231*, 1049−1067.
(59) Moran, R. G., Baldwin, S. W., Taylor, E. C., and Shih, C. (1989) The 6S- and 6R-diastereomers of 5,10-dideaza-5,6,7,8-tetrahydrofolate are equiactive inhibitors of de novo purine synthesis. *J. Biol. Chem. 264*, 21047−21051.
(60) Matherly, L. H., and Goldman, D. I. (2003) Membrane transport of folates. *Vitam. Horm. (London, U.K.) 66*, 403−456.
(61) Moran, R. G. (1999) Roles of folylpoly-γ-glutamate synthetase in therapeutics with tetrahydrofolate antimetabolites: An overview. *Semin. Oncol. 26*, 24−32.
(62) Wildman, S. A., and Crippen, G. A. (1999) Prediction of Physicochemical Parameters by Atomic Contributions. *J. Chem. Inf. Comput. Sci. 39*, 868−873.
(63) Ferone, R., Hanlon, M. H., Singer, S. C., and Hunt, D. F. (1986) α-Carboxyl-linked glutamates in the folylpolyglutamates of *Escherichia coli*. *J. Biol. Chem. 261*, 16356−16362.
(64) Ferone, R., Singer, S. C., and Hunt, D. F. (1986) In vitro synthesis of α-carboxyl-linked folylpolyglutamates by an enzyme preparation from *Escherichia coli*. *J. Biol. Chem. 261*, 16363−16371.
(65) Moran, R. G. (1983) Characterization of the function of mammalian folylpolyglutamate synthetase (FPGS). *Adv. Exp. Med. Biol. 163*, 327−339.
(66) Klein, C., Chen, P., Arevalo, J. H., Stura, E. A., Marolewski, A., Warren, M. S., Benkovic, S. J., and Wilson, I. A. (1995) Towards structure-based drug design: Crystal structure of a multisubstrate adduct complex of glycinamide ribonucleotide transformylase at 1.96 Å resolution. *J. Mol. Biol. 249*, 153−175.
(67) Marsilje, T. H., Hedrick, M. P., Desharnais, J., Tavassoli, A., Zhang, Y., Wilson, I. A., Benkovic, S. J., and Boger, D. L. (2003) Design, synthesis, and biological evaluation of simplified α-Keto heterocycle, trifluoromethyl ketone, and formyl substituted folate analogues as potential inhibitors of GAR transformylase and AICAR transformylase. *Bioorg. Med. Chem. 11*, 4487−4501.
(68) Lovelace, L. L., Minor, W., and Lebioda, L. (2005) Structure of human thymidylate synthase under low-salt conditions. *Acta Crystallogr. D61*, 622−627.
(69) Dixon, M. M., Huang, S., Matthews, R. G., and Ludwig, M. (1996) The structure of the C-terminal domain of methionine synthase: Presenting S-adenosylmethionine for reductive methylation of B12. *Structure 4*, 1263−1275.
(70) Szebenyi, D. M., Liu, X., Kriksunov, I. A., Stover, P. J., and Thiel, D. J. (2000) Structure of a murine cytoplasmic serine hydroxymethyltransferase quinonoid ternary complex: Evidence for asymmetric obligate dimers. *Biochemistry 39*, 13313−13323.
(71) Pejchal, R., Sargeant, R., and Ludwig, M. L. (2005) Structures of NADH and CH_3-H_4folate complexes of *Escherichia coli* methylenetetrahydrofolate reductase reveal a spartan strategy for a ping-pong reaction. *Biochemistry 44*, 11447−11457.
(72) Assaraf, Y. G. (2007) Molecular basis of antifolate resistance. *Cancer Metastasis Rev. 26*, 153−181.
(73) Wang, Y., Zhao, R., and Goldman, I. D. (2003) Decreased expression of the reduced folate carrier and folypolyglutamate synthetase is the basis for acquired resistance to the pemetrexed antifolate (LY231514) in an L1210 murine leukemia cell line. *Biochem. Pharmacol. 65*, 1163−1170.
(74) McCloskey, D. E., McGuire, J. J., Russell, C. A., Rowan, B. G., Bertino, J. R., Pizzorno, G., and Mini, E. (1991) Decreased folylpolyglutamate synthetase activity as a mechanism of methotrexate resistance in CCRF-CEM human leukemia sublines. *J. Biol. Chem. 266*, 6181−6187.
(75) Liani, E., Rothem, L., Bunni, M. A., Smith, C. A., Jansen, G., and Assaraf, Y. G. (2003) Loss of folylpoly-γ-glutamate synthetase activity is a dominant mechanism of resistance to polyglutamylation-dependent novel antifolates in multiple human leukemia sublines. *Int. J. Cancer 103*, 587−599.
(76) Desmoulin, S. K., Hou, Z., Gangjee, A., and Matherly, L. H. (2012) The human proton-coupled folate transporter: Biology and therapeutic applications to cancer. *Cancer Biol. Ther. 13*, 1355−1373.
(77) Gonen, N., and Assaraf, Y. G. (2012) Antifolates in cancer therapy: Structure, activity and mechanisms of drug resistance. *Drug Resist. Updates 15*, 183−210.
(78) Deng, Y., Wang, Y., Cherian, C., Hou, Z., Buck, S. A., Matherly, L. H., and Gangjee, A. (2008) Synthesis and discovery of high affinity folate receptor-specific glycinamide ribonucleotide formyltransferase inhibitors with antitumor activity. *J. Med. Chem. 51*, 5052−5063.
(79) Cherian, C., Kugel Desmoulin, S., Wang, L., Polin, L., White, K., Kushner, J., Stout, M., Hou, Z., Gangjee, A., and Matherly, L. H. (2013) Therapeutic targeting malignant mesothelioma with a novel 6-substituted pyrrolo[2,3-d]pyrimidine thienoyl antifolate via its selective uptake by the proton-coupled folate transporter. *Cancer Chemother. Pharmacol. 71*, 999−1011.
(80) Habeck, L. L., Leitner, T. A., Shackelford, K. A., Gossett, L. S., Schultz, R. M., Andis, S. L., Shih, C., Grindey, G. B., and Mendelsohn, L. G. (1994) A novel class of monoglutamated antifolates exhibits tight-binding inhibition of human glycinamide ribonucleotide formyltransferase and potent activity against solid tumors. *Cancer Res. 54*, 1021−1026.